Published in Proceedings of the 6th International Conference on Pattern Recognition Applications and Methods (ICPRAM 2017), 442-447. doi:10.5220/0006191504420447

Oil Spill Detection using Segmentation based Approaches

D. Mira[1], P. Gil[2], B. Alacid[1], and F. Torres[2]
[1] *Computer Science Research Institute, University of Alicante, Alicante, Spain*
[2] *Dept. of Physics, Systems Engineering and Signal Theory, University of Alicante, Alicante, Spain*
{damian.mira, pablo.gil, bea.alacid, fernando.torres}@ua.es

Keywords: Oils Spill Detection, Remote Sensing, Segmentation, SLAR Data.

Abstract: This paper presents a description and comparison of two segmentation methods for the oil spill detection in the sea surface. SLAR sensors acquire video sequences from which snapshots are extracted for the detection of oil spills. Both approaches are segmentation based on graph techniques and J-image respectively. Finally the aim of applying both approaches to SLAR snapshots, as shown, is to detect the largest part of the oil slick and minimize the false detection of the spill.

1 INTRODUCTION

Year on year, the increase in traffic of goods and people has resulted in the proliferation of cargo and passenger ships. This has placed pressure on maritime surveillance to deal quickly and effectively with marine mishaps. Surveillance is necessary to prevent bad practices that lead to water pollution, such as the illegal tank cleaning of ships. The maritime surveillance requires the use of information from different types of sensors in different locations. These sensors can be located on satellites, as SAR (Synthetic Aperture Radar), or on board, such as SLAR (Side Looking Airborne Radar) and thermal sensors or transponders.

The biggest problem in marine pollution is oil spills. Cases like the Prestige (García-Mira et. al. 2006) and the oil drilling dig of the Gulf of Mexico, (Ramseur 2010), exemplify the problems of these large-scale disasters. But it is not only the large-scale disasters that have a damaging impact on eco-systems. An example of a lesser magnitude spill is the sinking of the ship Oleg Naydenov, 15 miles south of Punta Maspalomas (Gran Canaria, Spain), which presented a threat to the ecosystem and it was also in a touristic zone.

The demand to control oil spills, has resulted in numerous studies for the detection, monitoring and controlling of such discharges on the sea surface. SAR sensors are used to provide information in the majority of studies which autonomously carry out the task of detecting oil spills (Topouzelis, 2008). The widespread use of these radars is due to their attributes, such as invariance to different climatic conditions, clouds, day/night and so forth. On the contrary, these radars have some features which perturb the detection of oil spills on the sea surface; among them can be highlighted, the wind speed at the surface (Brekke and Solberg, 2005), the presence of accumulations of marine plankton that causes false positives (Blondeau-Patissier et. al. 2014) or the presence of layers of floating ice (Brekke et. al. 2014). SAR are mounted at satellites and they present some disadvantages such as the satellite must be in the proper orbit to scan a specific area and, therefore, both the necessary response time and the need for emergency action are hampered.

There is a scarcity of studies using SLAR technology whose objective is oil spill detection. Nevertheless, for detecting oil spills from the information acquired by SAR radars, various techniques have been documented, such as artificial intelligence (Singha et.al. 2012), statistical and mathematical techniques (Li and Li, 2010), information extraction from features in image (Hu and Xiao, 2013) among others. Therefore, in this paper we present below some examples of solutions based on segmentation processes using features in image.

Thus, (Solberg et al. 2007) presented an oil spill detection algorithm based on segmentation by

adaptive thresholding and Gaussian pyramids, and extraction of features from the image for classification. The shown success rate in that work was between 72% and 77% accuracy in the detection of oil slicks. Authors as (Mera et al., 2012) proposed an algorithm with an adaptive thresholding from a calibration of the images to represent in each pixel the reflection backscatter of the radar, and the estimation of the wind in the sea surface. The aforementioned authors add to the previous work a characterization algorithm oriented to the classification of contour shapes of the regions labelled as oil spill (Mera et al., 2014). Others authors in (Chang et. al., 2008) showed a method based on clustering and region segmentation. The segmentation was done by a technique based on the moment preservation. This method splits the image in regions with similar moment. Later, the neighbour regions are combined with the N-nearest-neighbour rule by the spatial correlation data of each region. A data model of the oil spill is built with the segmentation results, which is approximated by the use of normal distributions. Finally a Generalized Likelihood Ratio Test (GLRT) is used to identify the oil spills.

Another methodology used for the detection of oil spills was that proposed (Shu et al., 2010) in which the spatial density was used, (defined by the quantity of pixels in an area with an intensity value), which is selected as it is likely to indicate an oil spill. To do this, initially a Gaussian smooth with a 3x3 mask and a standard deviation of 0.5 is done. Then, a segmentation based on an intensity thresholding by Otsu was performed. Subsequently, a second segmentation process, in which the threshold is the density of the pixels considered as a spill, is carried out for the detection. Finally, a filter was applied in order to avoid false positives by determining the significant region pixels according to their area and contrast.

2 AIRBONE SENSORY SYSTEM

The sensor used (SLAR) is an airborne radar, whose technology is similar to the synthetic aperture radar, SAR. Some differences between SAR and SLAR exist in the identification of two scanning zones by the SLAR: the blind zone of sensor, and the valid area for data processing as shown in Figure 1. In (Alacid and Gil, 2016), the authors proposed a method to solve the problem of identifying the blind zone of the sensor and other disturbances which cause noise, as aircraft turns, using image processing techniques without other information as altimeter, inclinometer and so forth.

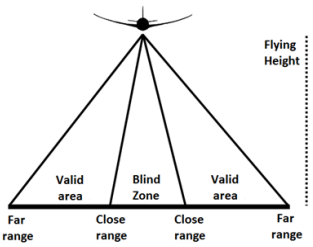

Figure 1. Diagram of scan areas of the SLAR.

3 SEGMENTATION OF OIL SPILLS

The first approach of our work was based on testing some well-known techniques of adaptive thresholding similar to (Liu et. al., 2011) as well as some saliency map algorithms as in (Jiang et. al., 2013). It did not yield satisfactory results in terms of correctly identify the region with oil spills. Moreover, this last algorithm presents a high computation cost and over-segmentation in the region of the spot.

3.1 Previous Filter of the Image

In order to solve the problems presented in the methods previously commented, two new approaches have been implemented, one, graph-based segmentation and another segmentation based on J-image.

In both methods a pre-processing step is performed, after the process of identification of the blind zone sensor and turns of the aircraft (Alacid and Gil, 2016). This pre-processing is performed to remove noise in the area of the selected snapshot and highlight areas which may potentially represent oil spills (Figure 2a). For this, a Gaussian filter is used and subsequently an analysis of the shape and values of the histogram is done to perform an equalization. This allows us to enhance the contrast in order to eliminate the outliers of high and low intensity, amounting to around 2%. Subsequently, a process is performed to manually remove borders of certain areas in the image that could be indicative of oil spill regions, although in fact they do not represent oil spills. Thus the pixels of these unrepresentative areas are homogenized or otherwise, they are reduced to make them less representative, resulting in a more accurate detection of other regions that may contain oil spills (Figure 2b).

3.2 Gray Level Co-occurrence Matrix

The proposed segmentation methods use co-occurrence matrix to improve the image processing and enhance the detection process. The Gray Level Co-occurrence Matrix, (GLCM) is commonly used to mathematically measure textures in the image (Haralick, 1979). This matrix approximates the joint probability distribution of a pair of pixels. Thus, it describes the frequency by which a gray level is displayed in a specific spatial relationship to another gray value within the specified window.

Within the values that can be obtained through GLCM, the values of energy (1), and correlation (2) have been used.

$$\sum_{i,j=0}^{N-1} {P_{i,j}}^2 \tag{1}$$

$$\sum_{i,j=0}^{N-1} P_{i,j} \left[\frac{(i-\mu_i)(j-\mu_j)}{\sqrt{(\sigma_i{}^2)(\sigma_j{}^2)}} \right] \tag{2}$$

where $P_{i,j}$ is the probability of co-occurrence of gray values for i, j, where i is the position in the row and j the position on the column. N represents the size of the window, μ the mean for i and j, and σ variance for i and j.

The result of applying these values to the pre-processed image can be seen in Figure 2c-d.

3.3 Graph based Segmentation

Given the need for a robust segmentation in which the non-homogeneity is taken into account for proper segmentation, the graph-based segmentation method is implemented (Felzenszwalb and Huttenlocher, 2004), which improves the detection process of regions representing spots, whose pixels maintain a distribution of varying intensity on SLAR images with progressive intensity gradients. The progressive intensity gradients in the image represent the loss of the sensor sensitivity, dependent on the resolution range (3),

$$R_r = \frac{c_0 t_p}{2 \sin \gamma} \tag{3}$$

where γ is the angle of incidence of radar on the scanned portion, c_0 is the speed of light and t_p the pulse duration. This data are restricted to the authors, because they do not have access to SLAR calibration. The resolution range is determined by the value of the incidence angle of sensor, so each pixel at near borders represents a larger portion of scanning field than the pixels of the centre of the image.

In addition, these gradients are exacerbated by the problem of dissolution of the spill, due to weather conditions and time. Some of the tests consisted in applying to this algorithm some modifications in order to address the problem, by modifying the internal management of vectors which stores the characteristics of intensity values of the pixels of the scanned region.

The operation of this method is based on four major steps. First, each pixel (i, j) of the image is read and it is stored in a vector of differences of intensity values for its four neighbour pixels (i + 1, j), (i, j + 1), (i +1, j + 1) and (i + 1, j-1). Then, this vector is ordered by the difference value from lowest to highest. In the second step, the vector is read and the pixels are added to a disjoint-set depending on whether the difference among pixels is less than the threshold defined at the outset. Thus, a disjoint-set characterization in which its pixels are grouped according to the difference among its four neighbours is obtained. This feature provides the algorithm with the ability to identify intensity degradation areas as only one region. The third step of the method involves removing groups of pixels with a smaller size than those used at the outset in the algorithm. Finally, a labelling of the generated tree is done to obtain the binary matrix with the performed segmentation. An example of the result of applying this algorithm can be seen in Figure 3a.

3.4 J-Image Segmentation

A J-image (Deng and Manjunath, 2001) is one in which each element in the picture is defined, firstly, by its intensity obtained as the mean difference of variance of all tonalities of intensity within a neighbourhood environment or window, and, secondly, by the relative position of these tones in relation to the central pixel of the window. To perform this segmentation a normalization process of the image must be made in which gray levels are reduced, as done with the aforementioned co-occurrence matrix.

J-image is obtained as follows:

$$J = (S_T - S_W)/S_W \tag{4}$$

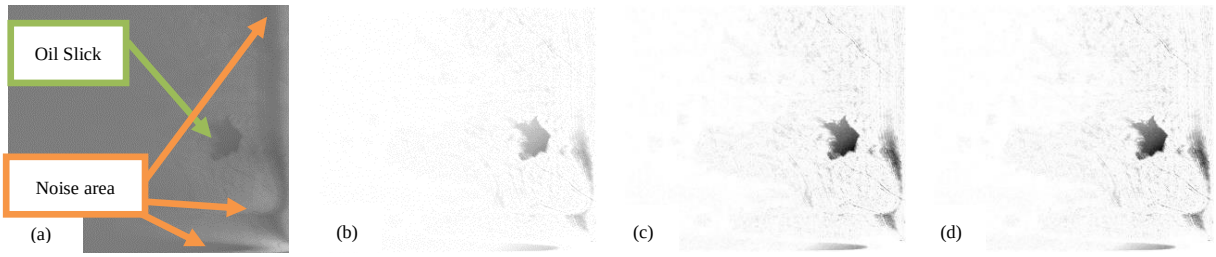

Figure 2. a) Original snapshot. b) Pre-processed image. c) Energy image. d) Correlation image.

For this, first it is performed an image transformation at N gray scales, each gray scale is taken as a class.

With these values the total variance is calculated as:

$$S_T = \sum_{z \epsilon Z} \|z - \bar{z}\|^2 \qquad (5)$$

where Z are all pixels of the normalized image, so that z = (i, j) in which $z \in Z$, $\bar{z}$ is the average coordinate of the elements of Z. Next, the mean of variance of each class is calculated as:

$$S_W = \sum_{i=1}^{C} S_i = \sum_{i=1}^{C} \sum_{z \in Z_i} \|z - \bar{z}_i\|^2 \qquad (6)$$

where $\bar{z}_i$ is the average coordinate Z_i class and C is the number of gray levels used in the normalization. Once the J-image is obtained, the segmentation is performed using as seed pixels the J value less than the selected threshold, obtaining the final result shown in Figure 3b.

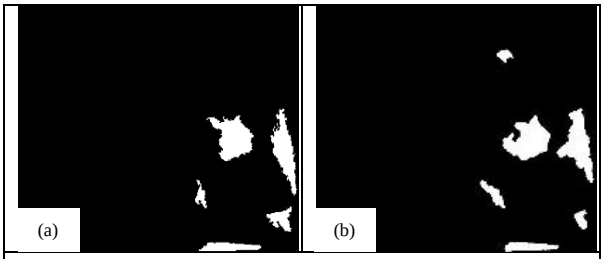

Figure 3. a) Graph-based segmentation for the Figure 2b image. b) J-image segmentation for the Figure 2b image.

4 RESULTS AND ANALYSIS

To analyse the success rate of developed segmentation methods, a ground truth from the original images is created in which the oil spill region is manually extracted, obtaining an image with the oil spill area represented by white pixels and the rest of the image is represented by black pixels.

The objective of this work is to maximize the True Positive rate, TP, which corresponds to the well-segmented pixels which are part of the oil spill. Additionally, another objective is to reduce the False Positive rate, FP, which represents the erroneously detected pixels. The last region of pixels taken into account in this work is the False Negative rate, FN, which represents the non-detected pixels part of the oil spill. An example of these areas can be seen in Figure. 4, in which the oil spill is represented by the union of both TP and FN, the region segmented is represented by the union of the zones TP and FP.

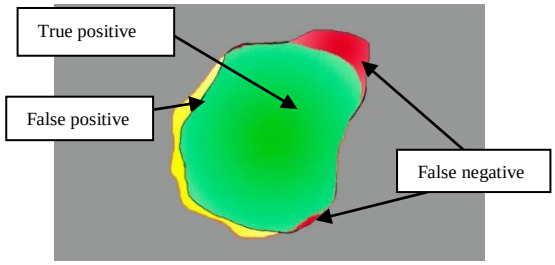

Figure 4. Example of representation of the zones labelled for the analysis of detection.

Table 1 shows the results for the true positive rate and false positive rate. It must be considered that both the J-image segmentation for the pre-processed image and the graph-based segmentation for the original image present a high percentage of false detection. Meanwhile, in the results with GLCM values, energy and correlation are more consistent, showing a difference of 1% between the J-image and the graph-based segmentation. Another issue to consider is the high standard deviation between the J-image and the graph-based segmentation. Graph-based segmentation has

Table 1. Accuracy rate of true and false positives from the snapshot of a video sequence ($t_1 \ldots t_n$) and for each scanning sequence t_i.

	Snapshot from video sequence $t_1 \ldots t_n$				From each scanning sequence t_i			
	TP (True Positive)		FP (False Positive)		TP (True Positive)		FP (False Positive)	
Image Type	J-Image	Graph	J-Image	Graph	J-Image	Graph	J-Image	Graph
Original	20.14%	73.97%	1.61%	27.46%	35.81%	85.30%	1.90%	26.96%
Pre-processed	92.03%	93.30%	14.42%	1.91%	81.16%	92.98%	15.19%	2.20%
Energy	90.34%	94.21%	2.48%	3.38%	80.16%	91.19%	2.78%	3.73%
Correlation	88.85%	95.40%	2.46%	3.11%	76.59%	93.21%	2.78%	3.44%

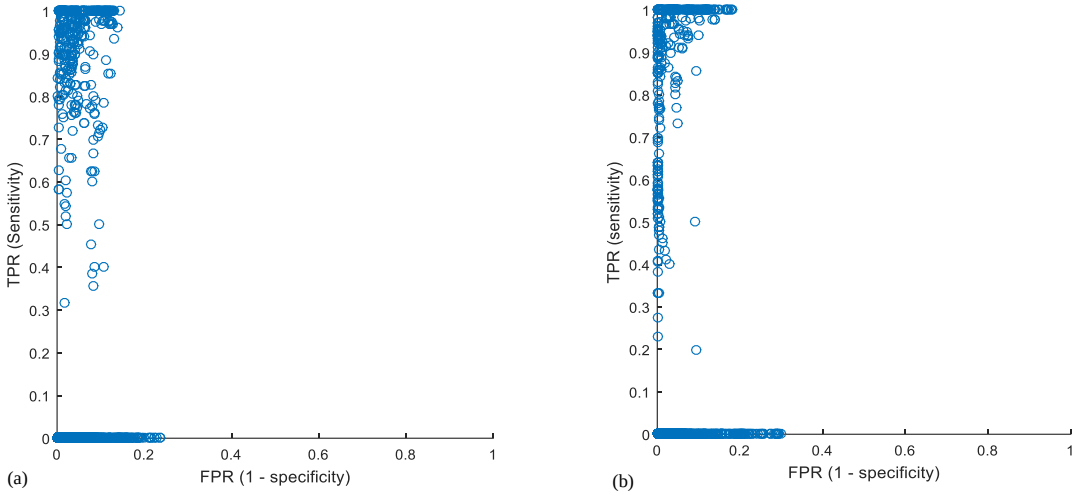

Figure 5. Example of ROC spaces for the scanning sequences. a) ROC space for the grap-based segmentation method with the GLCM energy, b) ROC space for the J-image segmentation with the GLCM energy.

approximately twice the standard deviation value of J-image.

Table 1 additionally shows the result for the true positive rate and false positive rate, when the algorithms are used with successive sequences of scanning, each time with the results of the SLAR sensor. Thereby, it can be seen that the FP rate is similar to that previously obtained, but it is higher using scanning sequences, than the static snapshots generated from the video sequences. In the results for the true positive rate, a high difference can be seen between the results obtained for the TP shown in Table 1.

Finally, for scanning sequences, Figure 5 shows the results for ROC space of graph-based segmentation and J-image segmentation. In both cases, some detection problems are still present. These problems correspond to the sequences where there is nothing to segment but some segmentation data is obtained. Although these bad results seem to be high, they are made up by less than 10% of the total results.

5 CONCLUSIONS

According to the results obtained in Section IV, the graph-based segmentation is valid for the detection of regions that may contain oil spills, but it generates high percentages of false positive detection in non-connected regions. Furthermore, the J-image segmentation method has a slightly lower successful rate for the TP rate than the other approach, but it obtains much lower false positive percentages in the segmentation process. Therefore, it enables us to keep more information on the oil slick. We can obtain features that describe the oil slick, such as compaction, perimeter, elongation and so forth. The best and most consistent results are obtained when it is applied the correlation value with the J-image segmentation using the static images generated from the acquisition and grouping of the scanning sequences of the SLAR.

Future objectives are focused on studying methods for the classification of the segmented regions which represent potential oil spill areas.

ACKNOWLEDGEMENTS

This work was funded by Ministry of Economy and Competitiveness and supported by Spanish project (RTC-2014-1863-8) Thanks to INAER Helicopters S.A.U. for provide the SLAR aerial data.

REFERENCES

Alacid, B., Gil, P., 2016. An approach for SLAR images denoising based on removing regions with low visual quality for oil spill detection. *SPIE Remote Sensing-Image and Signal Processing for Remote Sensing*, 26 - 29 September 2016, Edinburgh, United Kingdom.

Blondeau-Patissier, D., Gower, J. F., Dekker, A. G., Phinn, S. R., Brando, V. E, 2014. A review of ocean color remote sensing methods and statistical techniques for the detection, mapping and analysis of phytoplankton blooms in coastal and open oceans. *Progress in oceanography*, 123, 123-144.

Brekke, C., Solberg, A. H., 2005. Oil spill detection by satellite remote sensing. *Remote sensing of environment*, 95(1), 1-13.

Brekke, C., Holt, B., Jones, C., Skrunes, S., 2014. Discrimination of oil spills from newly formed sea ice by synthetic aperture radar. *Remote Sensing of Environment*, 145, 1-14.

Chang, L., Tang, Z.S., Chang, S.H., Chang, Y., 2008. A region-based GLRT detection of oil spills in SAR images, *Pattern Recognition Letters*, Volume 29, Issue 14, 15 October 2008, Pages 1915-1923, ISSN 0167-8655.

Deng, Y., Manjunath, B. S., 2001. Unsupervised segmentation of color-texture regions in images and video, *in IEEE Transactions on Pattern Analysis and Machine Intelligence*, vol. 23, no. 8, pp. 800-810, Aug 2001.

Felzenszwalb, P. F., Huttenlocher, D. P., 2004. Efficient graph-based image segmentation, *International Journal of Computer Vision*, vol. 59, no. 2, pp. 167-181.

García-Mira, R., Real, J.E., Uzzell, D.L., San Juan, C., Pol, E., 2006. Coping with a threat to quality of life: the case of the Prestige disaster, *Revue Européenne de Psychologie Appliquée/European Review of Applied Psychology*, Volume 56, Issue 1, March 2006, Pages 53-60, ISSN 1162-9088.

Haralick, R. M., 1979. Statistical and structural approaches to texture, *in Proceedings of the IEEE*, vol. 67, no. 5, pp. 786-804, May 1979.

Hu, G., Xiao, X., 2013. Edge detection of oil spill using SAR image. *Cross Strait Quad-Regional Radio Science and Wireless Technology Conference (CSQRWC)*, Chengdu, pp. 466-469.

Jiang, H., Wang, J., Yuan, Z., Wu, Y., Zheng, N., Li, S., 2013. Salient Object Detection: A Discriminative Regional Feature Integration Approach, *Computer Vision and Pattern Recognition (CVPR)*, 2013 IEEE Conference on, vol., no., pp.2083-2090, 23-28 June 2013.

Li, Y., Li, J., 2010. Oil spill detection from SAR intensity imagery using a marked point process, *Remote Sensing of Environment*, Volume 114, Issue 7, 15 July 2010, Pages 1590-1601, ISSN 0034-4257, http://dx.doi.org/10.1016/j.rse.2010.02.013.

Liu, P., Li, X., Qu, J.J., Wang, W., Zhao, C., Pichel, W., 2011. Oil spill detection with fully polarimetric UAVSAR data, *Marine Pollution Bulletin*, Volume 62, Issue 12, December 2011, Pages 2611-2618, ISSN 0025-326X.

Mera, D., Cotos, J.M., Varela-Pet, J., Garcia-Pineda, O., 2012. Adaptive thresholding algorithm based on SAR images and wind data to segment oil spills along the northwest coast of the Iberian Peninsula, *Marine Pollution Bulletin*, Volume 64, Issue 10, October 2012, Pages 2090-2096, ISSN 0025-326X.

Mera, D., Cotos, J.M., Varela-Pet, J., Rodríguez, P.G., Caro, A., 2014. Automatic decision support system based on SAR data for oil spill detection, *Computers & Geosciences*, Volume 72, November 2014, Pages 184-191, ISSN 0098-3004,

Ramseur, J. L. 2010. *Deepwater Horizon oil spill: the fate of the oil*. Washington, DC: Congressional Research Service, Library of Congress.

Shu, Y., Li, J., Yousif, H., Gomes, G., 2010. Dark-spot detection from SAR intensity imagery with spatial density thresholding for oil-spill monitoring, *Remote Sensing of Environment*, Volume 114, Issue 9, 15 September 2010, Pages 2026-2035, ISSN 0034-4257.

Singha, S., Bellerby, T. J., Trieschmann, O., 2012. Detection and classification of oil spill and look-alike spots from SAR imagery using an Artificial Neural Network, *IEEE International Geoscience and Remote Sensing Symposium*, Munich, 2012, pp. 5630-5633.

Solberg, A. H. S., Brekke, C., Husoy, P. O., 2007. Oil Spill Detection in Radarsat and Envisat SAR Images, *in IEEE Transactions on Geoscience and Remote Sensing*, vol. 45, no. 3, pp. 746-755, March 2007.

Topouzelis, K.N., 2008. Oil Spill Detection by SAR Images: Dark Formation Detection, Feature Extraction and Classification Algorithms. *Sensors* 2008, 8, 6642-6659.